Applied Catalysis B: Environmental 221 (2018) 618–625

Contents lists available at ScienceDirect

Applied Catalysis B: Environmental

journal homepage: www.elsevier.com/locate/apcatb

Water splitting over core-shell structural nanorod CdS@Cr_2O_3 catalyst by inhibition of H_2-O_2 recombination via removing nascent formed oxygen using perfluorodecalin

Bin Tian[a,b], Wei Gao[a,b], Xuqiang Zhang[a], Yuqi Wu[a,*], Gongxuan Lu[a,*]

[a] State Key Laboratory for Oxo Synthesis and Selective Oxidation Lanzhou Institute of Chemical Physics, Chinese Academy of Science, Lanzhou 730000, China
[b] University of Chinese Academy of Science, Beijing 100049, China

ARTICLE INFO

Keywords:
One-dimensional CdS@Cr_2O_3 core/shell nanorod catalyst
High efficient photogenerated charge separation and transfer
Suppression of the photocorrosion of CdS
Inhibition of the H_2-O_2 recombination reverse reaction
Photocatalytic hydrogen generation

ABSTRACT

One-dimensional CdS@Cr_2O_3 core/shell nanorod catalyst was prepared via one-step photodeposition for photocatalytic water splitting to hydrogen. The Cr_2O_3 shell was homogeneously coated on the surface of CdS/Pt core, forming coaxial heterostructure. This one-dimensional core/shell heterostructural assembly facilitates the high efficient photogenerated charge separation and transfer from CdS to Cr_2O_3 under visible light illumination, which suppressed the photocorrosion of CdS. Moreover, with the help of artificial blood component perfluorodecalin (PFDL), the nascent formed oxygen was removed from the reaction mixture, which further inhibited the oxygen induced photocorrosion, finally the catalyst exhibited 126.6 $\mu mol \cdot g^{-1}_{catalyst}$ H_2 formation in 2 h without sacrifice reagent addition under visible light irradiation. No significant decay of activity was observed in 8 h. The present results showed core-shell heterostructural CdS@Cr_2O_3 could be one of candidates for photocatalytic water splitting catalysts and oxygen capture reagent PFDL could be used for removing nascent oxygen to inhibit the H_2-O_2 recombination reverse reaction and enhance hydrogen evolution activity.

1. Introduction

Hydrogen is considered as an ideal energy storage medium and a promising energy carrier if it can be obtained from abundant natural resources such as water and biomass instead of fossil fuels. [1–16] In particular, photocatalytic water splitting is widely studied as a promising technology to produce hydrogen driven by solar light. [17–31] Over past 40 years various inorganic or organic semiconductors were studied, but it was mainly used in the half-reaction of water splitting (such as the water oxidation to O_2 or the proton reduction to H_2). [32–42] The difficulties of overall water splitting in pure water over a semiconductor are the low effective separation of photogenerated carriers, serious photocorrosion of some photocatalysts (especially CdS) and the rapid H_2-O_2 recombination reverse reaction, the latter was often neglected by researchers [43–49].

As we know, about 9.0 mg of oxygen can be dissolved in one liter of water at 20 °C and 100 kPa, while only very limited hydrogen can be dissolved in wtare under same condition. In addition, H_2 and O_2 recombination reaction is thermodynamic approved over many noble metal co-catalyst surfaces, leading to very fast reverse reaction of hydrogen and oxygen recombination over the photo-catalysts. [48] Therefore, remove the nascent O_2 from reaction system via oxygen transfer reagent is a necrssary to enchance hydrogen production. More recently, we achieved effectively hydrogen production over CdS/Pt/WO_3-CeO_x in pure water with the assisted of oxygen transfer reagent PFDL. [49] With help of PFDL, photocatalytic generated oxygen was captured by PFDL and transferred away from photocatalyst surface, then the backward reaction of water splitting was successfully restrained and the H_2 amount increased significantly. However, the separation efficiency of photogenerated carrier is still limited in this system.

Construction of a junction heterostructure between the narrow bandgap semiconductor shell and the wide bandgap semiconductor nanorod core is an effective strategy in improving the charge separation, which provides significant advantages both for light absorption and charge separation in photocatalyst. [50–53] Owing to these benefits, several types of core/shell heterostructural photocatalysts, such as TiO_2/CdS, ZnO/CdS_xSe_{1-x}, ZnO/$Zn_xCd_{1-x}Se$, ZnO/ZnS_xSe_{1-x} and TiO_2/CdS_xSe_{1-x} have been developed as potential candidates for solar energy conversion, which could absorb visible light and enhance the charge separation of photogenerated electrons and holes by transferring photoelectrons from shell to core. [54–58] However these heterosturctural

* Corresponding authors.
E-mail addresses: wuyuqicas@163.com (Y. Wu), gxlu@lzb.ac.cn (G. Lu).

http://dx.doi.org/10.1016/j.apcatb.2017.09.065
Received 27 July 2017; Received in revised form 23 September 2017; Accepted 26 September 2017
Available online 28 September 2017
0926-3373/

photocatalysts are difficult to overcome photocorrosion problem. Therefore, building a heterostructure with stable metal oxide shell over the surface of visible-light photocatalyst provides significant advantages both for charge separation and suppression of H_2-O_2 recombination. [59–62] At the same time, the photocorrosion and oxygen transfer problems might be improved.

Herein, we reported synthesis and excellent reaction activity of one-dimensional CdS@Cr_2O_3 core/shell nanorods photocatalyst for photocatalytic water splitting to hydrogen. The Cr_2O_3 shell was homogeneously coated on surface of CdS/Pt core, forming coaxial heterostructures. Such one-dimensional core/shell heterostructural catalyst facilitates the efficient photogenerated charge pair separation and the holes transfer from CdS to Cr_2O_3 under visible light illumination, which suppressed the photocorrosion of CdS. Moreover, with the help of artificial blood component perfluorodecalin (PFDL), our system achieved 126.6 $\mu mol \cdot g_{catalyst}^{-1}$ H_2 in 2 h without addition of sacrifice reagent under visible light irradiation and maintained excellent stability in 8 h without obvious decay. The present results imply that CdS@Cr_2O_3/Pt core/shell heterostructural catalyst is one of candidates for water splitting and capture oxygen reagent PFDL is a useful chemical to inhibit the H_2-O_2 recombination and enhance hydrogen evolution activity.

2. Results and discussion

The detailed preparation of photocatalysts and photocatalytic activity tests see Supporting Information. The XRD patterns (Fig. 1a) show appreciable sharp diffraction peaks, indicating high quality of crystallinity in all the photocatalyst samples. The diffraction patterns of CdS/Pt NRs were indexed to the hexagonal phase CdS (PDF#77-2306). The diffraction peaks center at 24.6°, 33.9°, 36.6°, 41.5° and 55.0° could be attributed to the hexagonal phase Cr_2O_3 (PDF#84-0315) in Cr_2O_3/Pt photocatalyst. Furthermore, compared to the CdS/Pt and Cr_2O_3/Pt photocatalyst, the CdS@Cr_2O_3/Pt photocatalyst show the diffraction peaks including CdS and Cr_2O_3 phase, indicated the CdS@Cr_2O_3/Pt photocatalyst was prepared successfully via photodeposition route in our experiment. However, no obvious diffraction peaks belonging to Pt were observed in all these photocatalyst probably due to very strong diffraction peaks of CdS NRs or Cr_2O_3 and the relatively small amount of Pt dispersed on composite photocatalyst. [63] Therefore, we prepared a CdS@Cr_2O_3/10%Pt sample for XRD. The data clearly show the characteristic diffraction peaks of PtNPs confirming that Pt has been successfully loaded on the photocatalyst (Fig. 1a).

The CdS@Cr_2O_3/Pt photocatalyst morphologies are then observed by transmission electron microscopy (TEM). As shown in Fig. 1b, the typical TEM image show that CdS had a rod structure with an average diameter of 50 nm, length of 100 nm and Cr_2O_3 wrapped in the surface of CdS with about 5 nm layer thickness. Moreover, the Pt nanoparticles (PtNPs) with a size of 3 nm mainly distribute in between CdS and Cr_2O_3. In order to clearly visualize the structure of our photocatalyst, the high resolution TEM (HRTEM) was used to investigate CdS@Cr_2O_3/PtNPs. As shown in Fig. 1c, the HRTEM image obviously show the lattice spacing of approximately 0.382 and 0.266, corresponding to the (002) plane of hexagonal CdS and (104) plane of hexagonal Cr_2O_3, respectively. [49,62] However, the no HRTEM image of PtNPs was observed in our system might attributed to the PtNPs was wrapped via Cr_2O_3 and this further confirm that Pt cocatalyst nanoparticles are anchored in between CdS and Cr_2O_3. Besides, the EDX data (Fig. 1d) show the existence of Cd, S, Pt, Cr and O, implying the CdS@Cr_2O_3 composite material was successfully built in our system. To further confirm the composition and element distribution of the photocatalysts, elemental mapping analysis was tested. The left image in Fig. 1e shows the TEM image of the region where elemental mapping was carried out. It was observed that all four elements existed in the photocatalysts and four elements (Cd, S, Cr, and O) uniformly dispersed in photocatalysts, and the distributional ranges of Cd, S, Cr and O elements were excellently overlapped, revealing that the CdS@Cr_2O_3 photocatalyst with core-shell structure formed in our system. Furthermore, the distribution of Pt elements was uniform dispersed in our photocatalyst. It further confirmed that the PtNPs formed and dispersed in the between Cr_2O_3 and CdS. These results are in good agreement with the results of XRD.

The presence chemical state of element in CdS@Cr_2O_3/Pt composite photocatalyst was further studied by X-ray photoelectron spectroscopy (XPS) (Fig. 2). The XPS survey spectrum shows the existence of Cd, S, Cr, O and Pt elements, as well as C 1 s (284.8 eV) as the reference. The high resolution XPS spectrum of Cd 3d (Fig. 2b) shows two peaks at Cd $3d_{5/2}$ (405.2 eV) and Cd $3d_{3/2}$ (411.9 eV), together with the S $2p_{3/2}$ (161.6 eV) and S $2p_{1/2}$ (162.8 eV) (Fig. 2c), which is the typical character of CdS. [49] After 8 h photo-reaction, the XPS spectra of Cd 3d and S 2p show no significant changes, indicating that CdS is stable and the system we built could effectively prevent photocorrosion problems of CdS nanorods. The scan spectrum of Cr 2p (Fig. 2d) shows two peaks at Cr $2p_{3/2}$ (577.4 eV) and Cr $2p_{1/2}$ (587.2 eV), together with the O 1s (530.9 eV) (Fig. 2e), which is the typical character of Cr_2O_3. [64] Additionally, the Pt $4f_{7/2}$ peak center in Fig. 2f at 70.9 eV suggested that K_2PtCl_6 indeed reduced to metallic PtNPs via photogenerated electrons which are consistent with the results of XRD. All these results confirmed the CdS@Cr_2O_3/Pt nanocomposite was prepared successfully and our photocatalytic system was stable by building the core-shell structure.

The effective absorption for sun light is a significant factor for an excellent photocatalyst on photocatalytic hydrogen evolution. Therefore, the spatial UV–vis diffused reflection absorption spectra were studied to examine the optical properties of CdS/Pt, Cr_2O_3/Pt and core-shell CdS@Cr_2O_3/Pt photocatalyst. As shown in Fig. 3a, the absorption of CdS@Cr_2O_3/Pt photocatalyst exhibited no significant change compared to CdS/Pt photocatalyst, indicated that the thickness of Cr_2O_3 is reasonable for photo-reaction. Moreover, the CdS@Cr_2O_3/Pt nanohybrid showed extra absorption at 600 nm consistent with the absorption of Cr_2O_3/Pt photocatalyst (Fig. S1), which is beneficial to enhance hydrogen evolution activity. Furthermore, the band gap (E_g) could be determined using the Eq. (1). [65]

$$(\alpha h\nu)^n = A(h\nu - E_g) \quad (1)$$

Where α is the absorption coefficient, $h\nu$ is the light energy, A is a constant, E_g is the optical band gap energy, and n is equal to 1/2 for an indirect band gap and 2 for a direct band gap. The transition of Cr_2O_3 and CdS is all indirect. [49,66] According to Eq. (1), the band gaps of the CdS/Pt and CdS@Cr_2O_3/Pt photocatalyst were estimated to be 2.25 and 2.32 eV from the onset of the absorption curves (Fig. 3b), respectively, which are consistent with the bulk values, indicating that the absorption range of CdS@Cr_2O_3/Pt photocatalyst was no significant change by wrapping Cr_2O_3 layers. Besides, the absorption spectra of Cr_2O_3/Pt clearly showed three peaks at 365, 460 and 600 nm indicated three prominent electronic transitions in Cr_2O_3/Pt sample. The observed peaks are consistent to earlier reports of Cr_2O_3. [67] The peak at about 365 nm is associated with the conventional band gap (~3 eV) of Cr_2O_3 (Fig. S2). [66] The absorption peaks at around 460 nm and 600 nm correspond to $4A_{2g} \rightarrow 4T_{1g}$ and $4A_{2g} \rightarrow 4T_{2g}$ $3d^3$ electronic transitions of octahedral Cr^{3+} ions. [68]

The band position is another important factor for water splitting over semiconductor. To study the band position of our photocatalysts and flat band potential, we subjected the CdS@Cr_2O_3/Pt nanocomposite photocatalyst to electrochemical impedance-potential spectroscopic analysis. The obtained Motte-Schottky plot is shown in Fig. 3c. Motte-Schottky plot of data analyzed using fitting method obey Ref. [69]. Experiment was carried out in 1.0 M H_2SO_4 solution at frequency of range from 10 to 2000 Hz within the potential region of −1.5 to 1.5 V vs SCE reference electrode. Variation of capacitance (C) with applied potential is shown by the Motte-Schottky Eq. (2): [70]

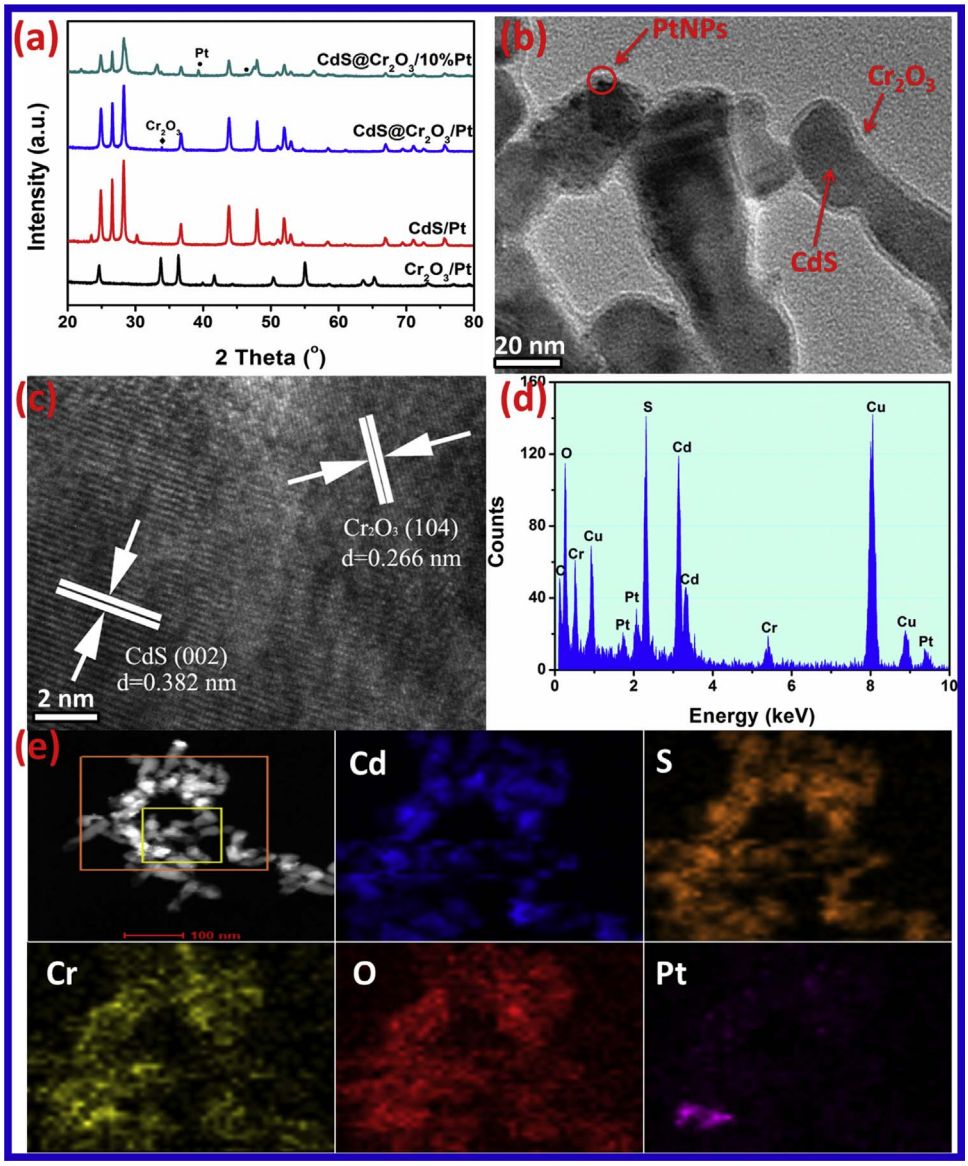

Fig. 1. (a) The XRD patterns of photocatalyst, (b) the TEM image of CdS@Cr_2O_3/Pt photocatalyst, (c) the HRTEM image of CdS@Cr_2O_3/Pt photocatalyst, (d) and (e) EDX spectra and TEM element mapping of CdS@Cr_2O_3/Pt photocatalyst.

$$\frac{1}{C^2} = \frac{2}{\varepsilon \cdot \varepsilon_0 \cdot e_0 \cdot A^2 \cdot N_D}(E - E_{FB} - \frac{kT}{e_0}) \quad (2)$$

where C is the space charge capacitance, ε and ε_0 are the permittivity of the electrode and free space, e_0 is the elementary charge, A is the electrochemical specific surface area, E is the applied potential, E_{FB} is the flat band potential, k is the Boltzmann's Constant and T is the temperature.

The negative slope of the plot confirms the *n*-type behavior of the CdS@Cr_2O_3/Pt, which is consistent with the result of CdS in the literature, and the flat-band potentials of photocatalysts calculated from the x intercepts of the linear region, is −0.56 V vs. NHE. (Fig. 3c). Generally, the potential measured against an SCE reference can be converted into reversible hydrogen electrode (NHE) potentials by using Eq. (3): [71]

$$E_{FB}(vs.RHE) = E_{FB}(SCE) + E_{SCE} + 0.059 \times pH \quad (3)$$

The measured pH value of the electrolyte is approximately 0, and E_{SCE} = 0.24 V. Therefore, the calculated flat-band positions of CdS@Cr_2O_3/Pt is −0.56 V vs. NHE (pH = 0), which is consistent with the results of UV-DRS. Therefore the corresponding conduction band (VB) and the valence band (CB) found at −0.56 V and 1.76 for CdS@Cr_2O_3/Pt vs normal hydrogen electrode (NHE). Based on above experiment result and analysis, it showed that the CdS@Cr_2O_3/Pt composite is a potential photocatalyst to split water into hydrogen and oxygen, simultaneously (Fig. 3d).

The photocatalytic behaviors of the CdS@Cr_2O_3/Pt catalyst with PFDL assist were carried out by measure the amount of H_2 evolution under visible light irradiation (λ > 420 nm). For comparison, the hydrogen production performances of CdS/Pt, Cr_2O_3/Pt and CdS@Cr_2O_3/Pt without PFDL were also investigated. As shown in Fig. 4a, it can be clearly seen that no appreciable H_2 was observed when Cr_2O_3/Pt was used under visible light irradiation (λ > 420 nm), revealing that Cr_2O_3/Pt is not an active photocatalyst, which could be the rapid recombination of photogeneratd carriers. In contrast, after CdS NRs introduced into Cr_2O_3/Pt system, the CdS@Cr_2O_3/Pt photocatalyst exhibited an obvious H_2 evolution activity, which could be interpreted to the effective separation of photoproduction carrier by core-shell structure of CdS and Cr_2O_3. [72] Interestingly, the hydrogen evolution enhanced significant after incorporation PFDL, indicated that the generated oxygen could be effective captured via PFDL and inhibited the recombination of generated hydrogen and oxygen, increased hydrogen evolution activity, subsequently.

In our recenty reported, we have demonstrated the activation energy of H_2 and O_2 recombination reaction is 16.5 kJ/mol regardless of

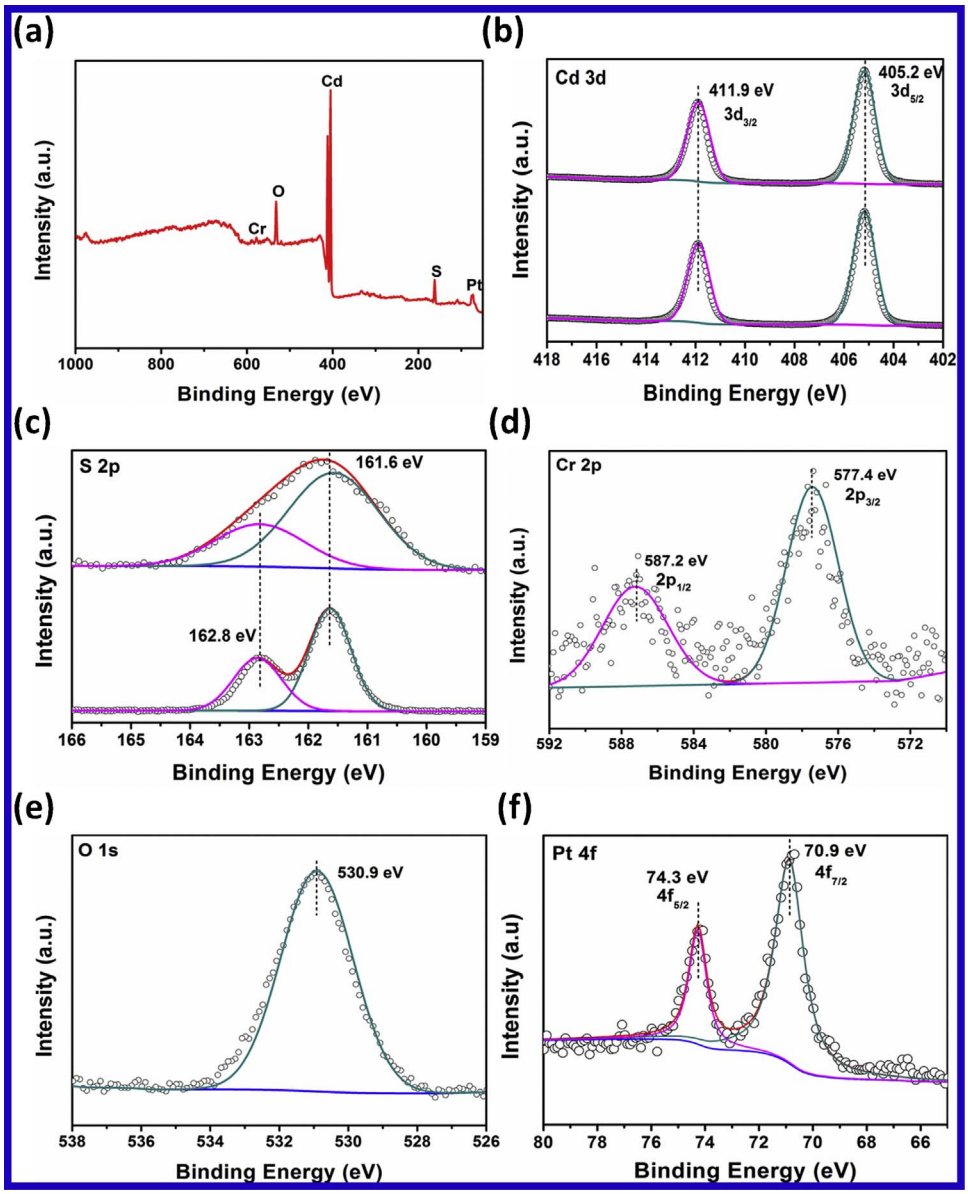

Fig. 2. The XPS spectra of CdS@Cr_2O_3/Pt photocatalyst, (a) survey spectra, (b) the Cd 3d scan spectra in CdS@Cr_2O_3/Pt photocatalyst, the before (under) and after (upper) reaction, (c) the S 2p scan spectra in CdS@Cr_2O_3/Pt photocatalyst, the before (under) and after (upper) reaction, (d) the Cr 2p scan spectra, (e) and (f) the O 1s and Pt 4f scan spectra.

light irradiation or not. [50] In this case, the photocatalytic evolved H_2 could react rapidly with the evolved O_2 to form H_2O again. This result indicates the backward reaction of overall water splitting is a thermal catalytic process and the H_2 and O_2 can recombinant without too much extra energy barrier, indicated that the backward reaction have a fatal effect on hydrogen evolution. In order to further elaborate the backward reaction of H_2 and O_2 to form H_2O also have an fatal effect on photocatalytic hydrogen evolution in our system, the recombination experiments of H_2 and O_2 were performed under dark. As shown in Fig. 4b, the injected stoichiometric H_2 and O_2 recombine rapidly over CdS@Cr_2O_3/Pt photocatalyst in a sealed Pyrex flask and detected H_2 decreased significantly, indicated clear H_2 and O_2 recombination reaction. Furthemore, the recombination experiments were carried out under the condition of irradiation and the result shown in Fig. S3. It clearly showed that the H_2-O_2 recombination reaction also have an adverse effect on hydrogen evolution. herefore, separating the generated H_2 and O_2 is one of the key and necessary factors to achieve the overall water splitting. These results is a solid evidence to explain the hydrogen production activity results and comfirmed our strategy is feasible to inhibite H_2 and O_2 recombination via PDFL, enhanced hydrogen evolution activity subsequently.

The isotopic tracer experiments were carried out to firmly identify H_2 and O_2 generated via water splitting in CdS@Cr_2O_3/Pt system, and the results were shown in Fig. 4c. The D_2O was used to prove the D_2 from water and results showed both D_2 and trace amount H_2 were detected, indicated the D_2 comes from water indeed. Furthermore, in order to account for O_2 also from water, the photocatalytic H_2O^{18} experiment was measured (Fig. 4d). The isotopes analysis results showed that $O_2{}^{18}$, and $O_2{}^{16}$ were all detected, indicating the O_2 also from water splitting. These results prove the H_2 and O_2 come from overall photocatalytic water splitting, and the PFDL here acts as O_2 transfer regent rather than sacrificing reagent.

In Fig. 5a, it showed the hydrogen evolution activity changed with the change of Cr_2O_3 layer thickness and the hydrogen evolution reach maximum when the concentration of $Cr(NO_3)_3$ is 1.0×10^{-4} mol/L. Further increase or decrease the amount of Cr^{2+} resulted in a decrease of the hydrogen evolution activity. It could be attributed to the thickness of Cr_2O_3 increased would decrease the absorption of sun light when the amount of $Cr(NO_3)_3$ is large. On the contrary, the Cr_2O_3 layer was thin would not effective inhibited CdS photocorrosion leaded to the low hydrogen evolution activity. Further experiments were performed to confirm the photocatalytic stability of the CdS@Cr_2O_3/Pt under

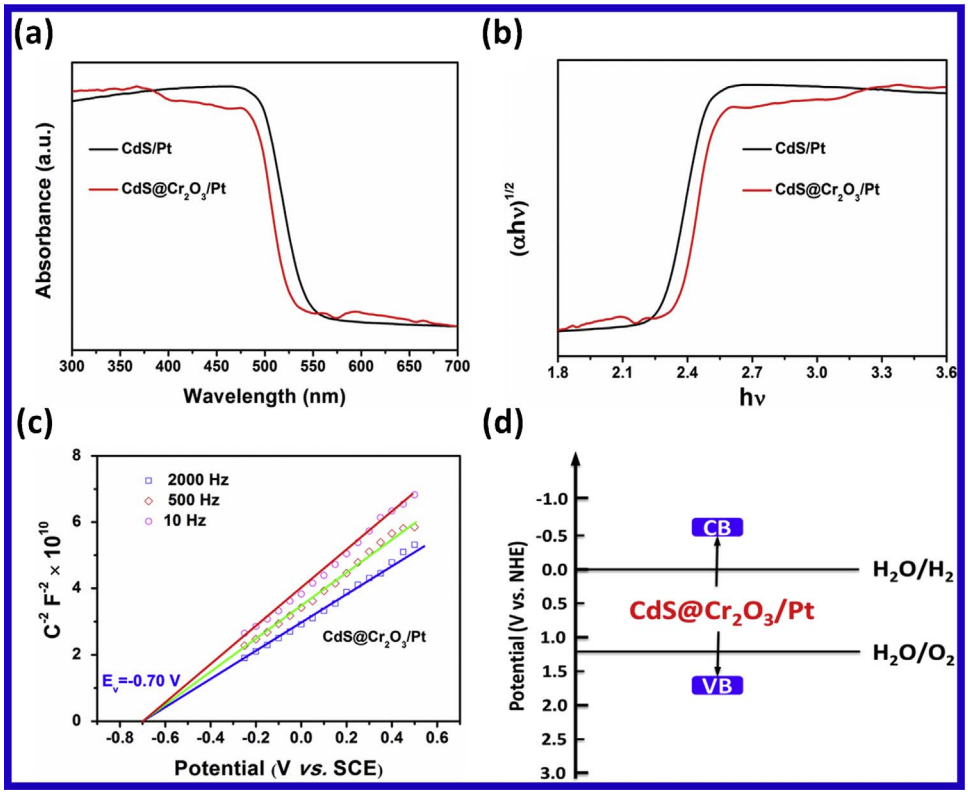

Fig. 3. (a) The UV–vis diffuse reflectance spectra of CdS/Pt and CdS@Cr_2O_3/Pt photocatalyst, (b) the band edge of CdS/Pt and CdS@Cr_2O_3/Pt photocatalyst, (c) Mott–Schottky plots for CdS@Cr_2O_3/Pt composites according to impedance measurements. The flat-band potentials are obtained from the intercepts of the extrapolated lines, (d) electronic potential diagram for CdS@Cr_2O_3/Pt in aqueous solutions.

visible light irradiation. The reaction system was evacuated every 120 min and the process was carried out for repeated cycles. As shown in Fig. 5b, there was no significant decrease in H_2 evolution through each cycle. The CdS@Cr_2O_3/Pt/PFDL photocatalytic system showed excellent stability and maintained a similar photocatalytic activity for more than 8 h, indicating good stability of this system for H_2 evolution and effectively overcome the corrosion problems of CdS, and there is no precipitate in our system after 8 h reaction by $BaCl_2$ detection. Moreover, we found the cadmium ion concentration in solution maintains essentially unchanged with light irradiation time and Cd^{2+} in solution

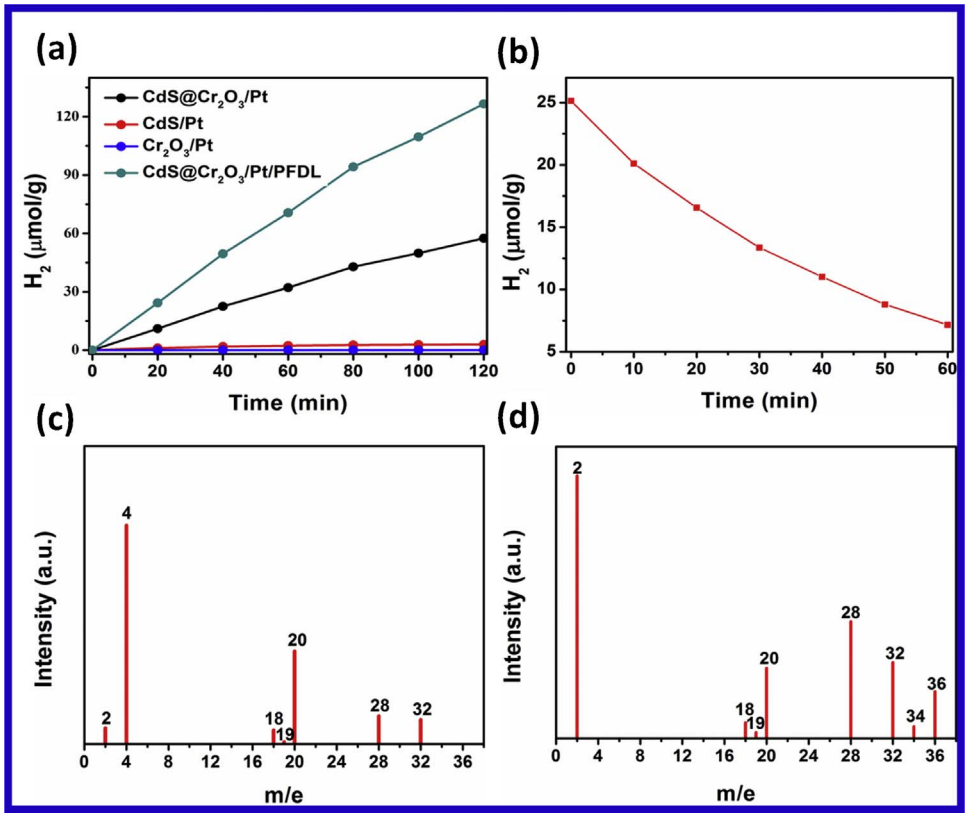

Fig. 4. (a) Comparison of photocatalytic H_2 evolution with different photocatalyst under visible light irradiation (λ > 420 nm) at room temperature. The system contains 50 mg photocatalyst, 100 mL deionized water, (b) The time courses of the H_2 and O_2 recombination reaction over CdS/Pt photocatalyst in a sealed Pyrex flask in dark at room temperature, (c) and (d) The GC–MS spectra obtained after injecting 0.5 mL samples of the gas phase species produced by D_2O or $H_2{}^{18}O$over CdS@Cr_2O_3/Pt photocatalyst in a sealed Pyrex flask during visible light irradiation 24 h (λ > 420 nm).

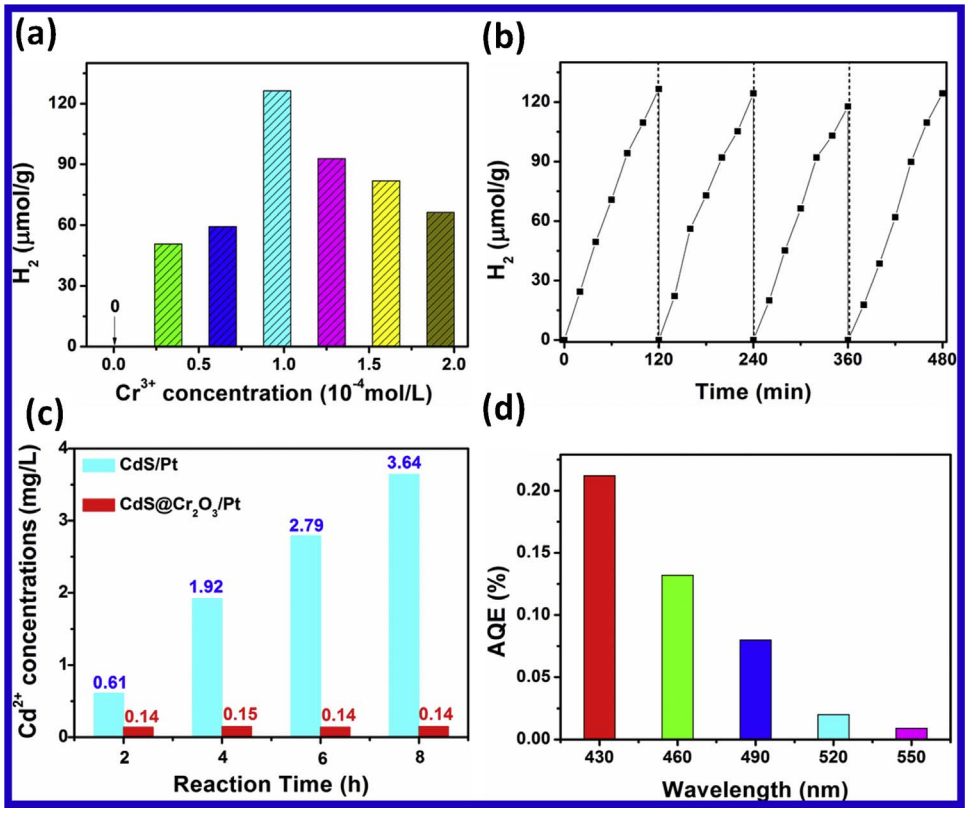

Fig. 5. (a) The hydrogen evolution activity with different Cr ion concentration, (b) the hydrogen production stability over $CdS@Cr_2O_3$/Pt photocatalyst, (c) the change of Cd^{2+} concentration in solution with reaction time, (d) the hydrogen evolution of AQE over $CdS@Cr_2O_3$/Pt photocatalyst, the wavelength of monochromatic light is 430, 460, 490, 520 and 550 nm.

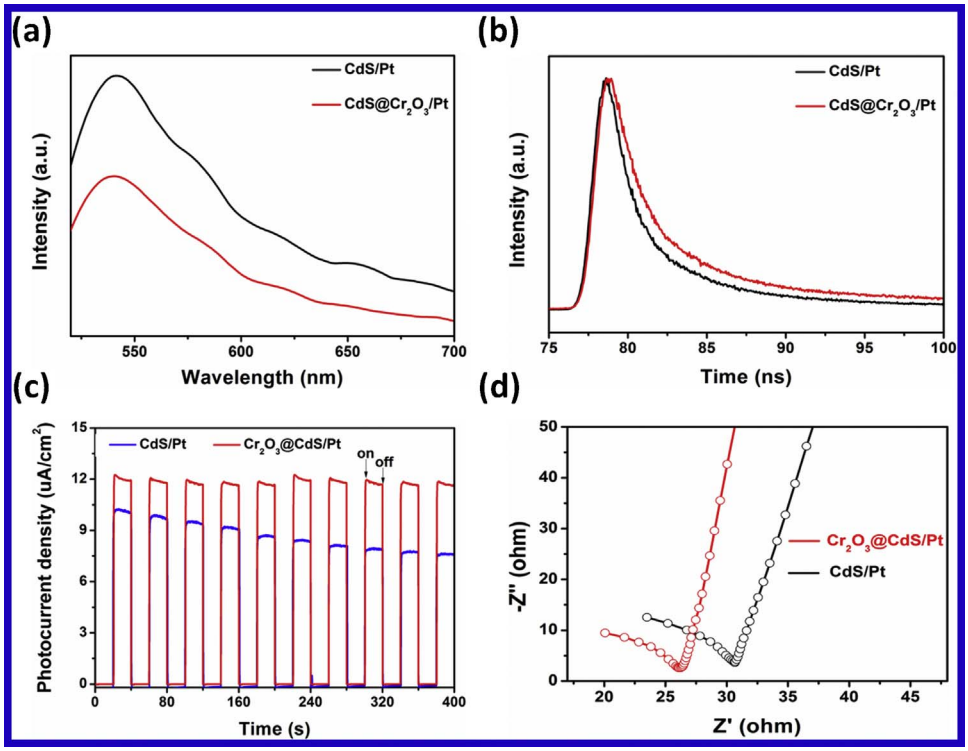

Fig. 6. (a) Photoluminescence spectra of photocatalyst at room temperature, (b) Time-resolved photoluminescence (TRPL) spectra of photocatalyst, the excitation wavelength was 464 nm, (c) transient photocurrent time profiles of photocatalysts on ITO glass in 0.5 M H_2SO_4 aqueous solution under visible light irradiation ($\lambda > 420$ nm), (d) EIS Nyquist plots of CdS/Pt and $CdS@Cr_2O_3$/Pt film electrodes.

was detected (Fig. 5c).

In addition, The apparent quantum efficiency (AQE) for H_2 production was next determined for the photocatalytic system containing 50 mg $CdS@Cr_2O_3$/Pt photocatalyst, 1 mL PFDL and 100 mL deionized water. The solution was irradiated with different wavelength visible light irradiation (λ = 430, 460, 490, 520 and 550 nm) and the result is shown in Fig. 5d. The highest AQE reached 0.22% after 60 min irradiation, which is agreement with UV–vis diffuse reflectance spectra results. Efficient conversion of visible light energy presumably suggests that the present $CdS@Cr_2O_3$/Pt/PFDL photocatalytic system is effective strategy for inhibiting H_2 and O_2 recombination and enchanced hydrogen evolution.

As compared with those reported in the literature, the aforementioned results show that the Cr_2O_3 wrapped CdS/Pt and PFDL system have excellent stability for photocatalytic H_2 evolution from pure water under visible light irradiation. Such stable and effective catalytic activity in our present work probably results from effectively transfered for photogenerated carriers, neogenesis oxygen and suppressed H_2 and O_2 recombination via core-shell structure and PFDL. The photocatalytic water splitting reaction in the photocatalysis system general can be divided into several fundamental processes, including visible light absorption by the semiconductor, generation of electron–hole pairs, electron–hole pair separation, and transfer of electrons to water which results in the formation of H_2 [73]. However, H_2 and O_2 recombination back-reaction problem also have a fatal effect, especially in the pure water system, which is often ignored by researchers and resulted in no net H_2 and O_2 evolution during irradiation in pure water system via many photocatalytic system. Previous experiment had illustrated the backward reaction had a fatal effect on water splitting, thereby separating the generated H_2 and O_2 is one of the key and necessary factors to achieve the overall water splitting.

To comfired that effective separation of photoproduction carrier and understand the reason for the drastically enhanced photocatalytic activity of CdS@Cr_2O_3 photocatalyst for H_2 evolution as compared to CdS NRs, we have further characterized these samples using photoluminescence (PL) spectra and timeresolved photoluminescence (TRPL) spectra, which are able to reflect the transfer of photogenerated charge carriers. Fig. 6a shows the PL data at an excitation wavelength of 464 nm, and two distinct emission bands at about 543 and 579 can be observed in CdS@Cr_2O_3/Pt system, which is in agreement with the previous reports. [74,75] Also, these emissions were remarkably quenched upon CdS@Cr_2O_3/Pt photocatalyst, attributing to the effective transfer of electrons from semiconductors to Pt cocatalyst, which can suppress the electron–hole recombination and enhance the photocatalytic activity. The transfer of photogenerated charge carriers of these samples has also been confirmed by the TRPL spectra. As shown in Fig. 6b, the TRPL data further indicated that the lifetime of CdS@Cr_2O_3/Pt was much shorter than that of CdS/Pt photocatalyst, also indicating the effective charge transfer. The decay curves were fitted with exponentials to obtain the decay time. The results showed the CdS NRs have two lifetimes which are 1.15 ns and 0.50 ns (Table S1). The short decay time component is considered to be due to quasi-free excitons, while the long component is attributed to localized exciton recombination, which are caused by de-trapping of carriers [49]. The CdS@Cr_2O_3/Pt photocatalyst have an average decay lifetime (0.83 ns), which could be the main influence on hydrogen evolution. [76] Photocatalysts with reduction cocatalyst materials are expected to have shorter lifetimes due to the efficient charge transfer from the photocatalyst to cocatalyst on the surface and suppression of the electron–hole recombination. The much decreased lifetime value of CdS@Cr_2O_3/Pt photocatalyst clearly indicates that our photocatalytic system is an effective strategy for the charge transfer. Furthermore, the photocurrent tests were performed and the result is shown in Fig. 6c. It is observed that the CdS@Cr_2O_3/Pt sample exhibited a highly enhanced photocurrent than CdS/Pt and Cr_2O_3/Pt photocatalyst under the same conditions, revealed the efficient charge transfer process in CdS@Cr_2O_3/Pt system, [77] which is consistent with the result of electrochemical impedance spectroscopy (EIS, Fig. 6d).

Based on above experiments and characterization analysis, the whole reaction process of photocatalysis overall water splitting over the CdS@Cr_2O_3/Pt/PFDL photocatalytic system can be explained in terms of Scheme 1. The semiconductor CdS and Cr_2O_3 absorbs visible light to excite the electrons from the valence band (VB) to the conduction band (CB). The photogenerated electrons transfer into the surface of PtNPs followed because of formative semicondouctor-metal junction between CdS and PtNPs. The electrons reduce H^+ to generate H_2 on the surface of PtNPs, while the H_2O was oxidized to form oxygen by the holes on the surface of Cr_2O_3. The generated H_2 and O_2 will recombinant rapidly

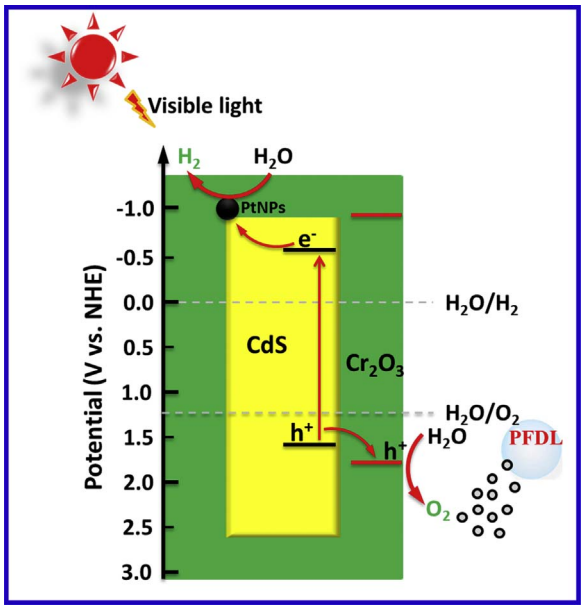

Scheme 1. The hydrogen evolution mechanism of CdS@Cr_2O_3/Pt/PFDL photocatalytic system.

to form water if there is no Cr_2O_3 layers and PFDL in the catalytic system. The generated O_2 was captured by PFDL because of PDFL possessed strong combination O_2 ability and eliminated from the system, subsequently, and inhibiting H_2 and O_2 recombination undesirable reaction. The PFDL can capture and transfer the newly generated O_2 and inhibit the H_2 and O_2 recombination backward reaction. Moreover, the photogenerated holes transfered from CdS into the Cr_2O_3 layers, effectively avoided CdS photocorrosion, leading to the continuous H_2 evolution.

3. Conclusion

In conclusion, one-dimensional CdS@Cr_2O_3 core/shell nanorods used as photocatalyst in hydrogen evolution reaction were prepared via one-step photodeposition. The Cr_2O_3 shell was homogeneously coated on the surface of CdS/Pt core, forming coaxial heterostructures. The one-dimensional core/shell heterostructure facilitates the photogenerated electron–hole pair separation and the holes transfer from CdS to Cr_2O_3 under visible light illumination, which suppressed the photocorrosion of CdS. Moreover, with the help of artificial blood component perfluorodecalin (PFDL), our system achieved 126.6 $\mu mol \cdot g^{-1}_{catalyst}$ H_2 in 2 h without sacrifice reagent under visible light irradiation and maintained excellent stability in 8 h without obvious decay. The present results imply that the recombination of CdS@Cr_2O_3/Pt core/shell heterostructure and capture oxygen reagent PFDL is a useful strategy to inhibit the H_2-O_2 recombination and enhance hydrogen evolution activity.

Conflict of interest

The authors declare no competing financial interest.

Acknowledgments

This work has been supported by the National Natural Science Foundation of China (Grant Nos. 21433007 and 21373245) and the 973 Program of Department of Sciences and Technology China (Grant Nos. 2013CB632404).

Appendix A. Supplementary data

Supplementary data associated with this article can be found, in the online version, at http://dx.doi.org/10.1016/j.apcatb.2017.09.065.

References

[1] H.B. Gray, Nat. Chem. 1 (2009) 7–7.
[2] N.S. Lewis, D.G. Nocera, Proc. Natl. Acad. Sci. 103 (2006) 15729–15735.
[3] Z.Y. Ma, X.B. Li, L.J. Deng, G. Fan, J. Mol. Catal. (China) 30 (2016) 575–582.
[4] C. Kong, Z. Li, G.X. Lu, Int. J. Hydrogen Energy 40 (2015) 5824–5830.
[5] Z. Li, C. Kong, G.X. Lu, Int. J. Hydrogen Energy 40 (2015) 9061–9068.
[6] C. Kong, Z. Li, G.X. Lu, Int. J. Hydrogen Energy 40 (2015) 9634–9641.
[7] W.L. Zhen, B. Li, G.X. Lu, J.T. Ma, Chem. Commun. 51 (2015) 1728–1731.
[8] W.Y. Zhang, C. Kong, G.X. Lu, Chem. Commun. 51 (2015) 10158–10161.
[9] Z. Li, Q.S. Wang, C. Kong, Y.Q. Wu, Y.X. Li, G.X. Lu, J. Phys. Chem. C 119 (2015) 13561–13568.
[10] W.Y. Zhang, G.X. Lu, Catal. Sci. Technol. 6 (2016) 7693–7697.
[11] J.H. Xiong, Y.H. Liu, S.J. Liang, S.Y. Zhang, Y.H. Li, L. Wu, J. Catal. 342 (2016) 98–104.
[12] B. Tian, Z. Li, W.L. Zhen, X.Q. Zhang, G.X. Lu, J. Catal. 352 (2017) 572–578.
[13] J.H. Alstrum-Acevedo, M.K. Brennaman, T.J. Meyer, Inorg. Chem. 44 (2005) 6802–6827.
[14] Z. Li, B. Tian, W.L. Zhen, W.Y. Zhen, X.Q. Zhang, Y.Q. Wu, G.X. Lu, Appl. Catal. B 219 (2017) 501–510.
[15] K. Maeda, K. Teramura, D.L. Lu, T. Takata, N. Saito, Y. Inoue, K. Domen, Nature 440 (2006) 295–295.
[16] G.X. Lu, B. Tian, J. Mol. Catal. (China) 31 (2017) 101–104.
[17] Z.X. Huang, Y.F. Li, Y.X. Li, X.Q. Huang, J. Mol. Catal. (China) 31 (2017) 181–187.
[18] W.J. Jiao, Y.Q. Wu, G.X. Lu, H.W. Jing, RSC Adv. 6 (2016) 29538–29544.
[19] W.L. Zhen, F. Gao, B. Tian, P. Ding, Y.B. Deng, Z. Li, H.B. Gao, G.X. Lu, J. Catal. 348 (2017) 200–211.
[20] W.L. Zhen, H.B. Gao, B. Tian, J.T. Ma, G.X. Lu, ACS Appl. Mater. Interfaces 8 (2016) 10808–10819.
[21] Y.P. Guo, G.X. Lu, Chinese J. Inorg. Chem. 32 (2016) 1177–1182.
[22] X.X. Zhao, G.X. Lu, J. Hydrogen Energy 41 (2016) 3349–3362.
[23] G.X. Lu, W.L. Zhen, J. Mol. Catal. (China) 31 (2017) 299–304.
[24] W.Y. Zhang, S.L. Yang, J. Li, W. Gao, Y.B. Deng, W.P. Dong, C.J. Zhao, G.X. Lu, Appl. Catal. B 206 (2017) 89–103.
[25] H.B. Gao, W.L. Zhen, J.T. Ma, G.X. Lu, Appl. Catal. B 206 (2017) 353–363.
[26] J.J. Hou, Q.H. Zhao, G. Li, P.W. Li, J. Hu, J. Mol. Catal. (China) 31 (2017) 258–266.
[27] Y.P. Guo, G.X. Lu, J. Hydrogen Energy 41 (2016) 6706–6712.
[28] W. Gao, W.Y. Zhang, G.X. Lu, Appl. Catal. B 212 (2017) 23–31.
[29] X.S. Huang, Y.X. Zhao, G.X. Lu, Z.C. Tang, J. Mol. Catal. (China) 31 (2017) 287–298.
[30] A. Kudo, Y. Miseki, Chem. Soc. Rev. 38 (2009) 253–278.
[31] F.E. Osterloh, Chem. Mater. 20 (2008) 35–54.
[32] B. Tian, W.L. Zhen, H.B. Gao, X.Q. Zhang, Z. Li, G.X. Lu, Appl. Catal. B 203 (2017) 789–797.
[33] W.Y. Zhang, C. Kong, W. Gao, G.X. Lu, Chem. Commun. 52 (2016) 3038–3841.
[34] B. Tian, Z. Li, W.L. Zhen, G.X. Lu, J. Phys. Chem. C 120 (2016) 6409–6415.
[35] S.X. Min, F. Wang, G.X. Lu, Catal. Commun. 80 (2016) 28–32.
[36] J. Suntivich, K.J. May, H.A. Gasteiger, J.B. Goodenough, Y. Shao-Horn, Science 334 (2011) 1383–1385.
[37] X.Q. Zhang, G.X. Lu, Carbon 108 (2016) 215–224.
[38] Z. Li, Y.Q. Wu, G.X. Lu, Appl. Catal. B 188 (2016) 56–64.
[39] W.L. Zhen, J.T. Ma, G.X. Lu, Appl. Catal. B 190 (2016) 12–25.
[40] Z. Li, B. Tian, W.L. Zhen, Y.Q. Wu, G.X. Lu, Appl. Catal. B 203 (2017) 408–415.
[41] Y. Lee, J. Suntivich, K.J. May, E.E. Perry, Y.J. Shao-Horn, J. Phys. Chem. Lett. 3 (2012) 399–404.
[42] X.C. Meng, Z.Z. Li, H.M. Zeng, J. Chen, Z.S. Zhang, Appl. Catal. B 210 (2017) 160–172.
[43] L. Jia, D.H. Wang, Y.X. Huang, A.W. Xu, H.Q. Yu, J. Phys. Chem. C 115 (2011) 11466–11473.
[44] X.F. Ning, J. Li, B.J. Yang, W.L. Zhen, Z. Li, B. Tian, G.X. Lu, Appl. Catal. B 212 (2017) 129–139.
[45] M. Wang, Z. Li, Y.Q. Wu, J.T. Ma, G.X. Lu, J. Catal. 353 (2017) 162–170.
[46] W. Gao, W.Y. Zhang, G.X. Lu, Appl. Catal. B 212 (2017) 23–31.
[47] W.L. Zhen, X.F. Ning, B.J. Yang, Y.Q. Wu, Z. Li, G.X. Lu, Appl. Catal. B 221 (2018) 243–257.
[48] Z. Li, B. Tian, W.L. Zhen, Y.Q. Wu, G.X. Lu, Appl. Catal. B 203 (2017) 408–415.
[49] B. Tian, B.J. Yang, J. Li, Z. Li, W.L. Zhen, Y.Q. Wu, G.X. Lu, J. Catal. 350 (2017) 189–196.
[50] Y.J. Hwang, A. Boukai, P.D. Yang, Nano Lett. 9 (2009) 410–415.
[51] H. Liu, J. Yuan, W.F. Shangguan, Y. Teraoka, J. Phys. Chem. C 112 (2008) 8521–8523.
[52] W.J. Fang, Z. Jiang, L. Yu, H. Liu, W.F. Shangguan, C. Terashima, A. Fujishima, J. Catal. 352 (2017) 155–159.
[53] B.Z. Tian, T.J. Kempa, C.M. Lieber, Chem. Soc. Rev. 38 (2009) 16–24.
[54] Y. Myung, D.M. Jang, T.K. Sung, Y.J. Sohn, G.B. Jung, Y.J. Cho, H.S. Kim, J. Park, ACS Nano 4 (2010) 3789–3800.
[55] T.K. Sung, J.H. Kang, D.M. Jang, Y. Myung, G.B. Jung, H.S. Kim, C.S. Jung, Y.J. Cho, J. Park, C.L. Lee, J. Mater. Chem. 21 (2011) 4553–4553.
[56] Y. Myung, J.H. Kang, J.W. Choi, D.M. Jang, J. Park, J. Mater. Chem. 22 (2012) 2157.
[57] Z.X. Wang, X.Y. Zhan, Y.J. Wang, M. Safdar, M.T. Niu, J.P. Zhang, Y. Huang, J. He, Appl. Phys. Lett. 101 (2012) 073105.
[58] K. Shin, S.H. Im, J.H. Park, Chem. Commun. 46 (2010) 2385–2387.
[59] T.F. Berto, K.E. Sanwald, J.P. Byers, N.D. Browning, O.Y. Gutierrez, J.A. Lercher, J. Phys. Chem. Lett. 7 (2016) 4358–4362.
[60] M. Yoshida, K. Takanabe, K. Maeda, A. Ishikawa, J. Kubota, Y. Sakata, Y. Ikezawa, K. Domen, J. Phys. Chem. C 113 (2009) 10151–10157.
[61] Y.J. Cho, G.H. Moon, T. Kanazawa, K. Maeda, W. Choi, Chem. Commun. 52 (2016) 9636–9639.
[62] N. Sakamoto, H. Ohtsuka, T. Ikeda, K. Maeda, D.L. Lu, M. Kanehara, K. Teramura, T. Teranishi, K. Domen, Nanoscale 1 (2009) 106–109.
[63] Z. Li, Q.S. Wang, C. Kong, Y.Q. Wu, Y.X. Li, G.X. Lu, J. Phys. Chem. C 119 (2015) 13561–13568.
[64] C. Xu, M. Hassel, H. Kuhlenbeck, H.J. Freund, Surf. Sci. 258 (1991) 1–3.
[65] M.M. Abdullah, F.M. Rajab, S.M. Al-Abbas, AIP Adv. 4 (2014) 027121.
[66] R.N. Bhowmik, K. Venkata Siva, R. Ranganathan, C. Mazumdar, J. Magn. Magn. Mater. 432 (2017) 56–67.
[67] T.C. Kaspar, P.V. Sushko, M.E. Bowden, S.M. Heald, A. Papadogianni, C. Tschammer, O. Bierwagen, S.A. Chambers, Phys. Rev. B 94 (2016) 155409.
[68] S. Lei, X. Peng, Z. Liang, X. Li, C. Wang, B. Cheng, Y. Xiao, L. Zhou, J. Mater. Chem. 22 (2012) 1643–1651.
[69] P. Shahbazi, A. Kiani, Int. J. Hydrogen Energy 41 (2016) 17247–17256.
[70] X.J. Zhu, T.M. Zhang, Z.J. Sun, H.L. Chen, J. Guan, X. Chen, H.X. Ji, P.W. Du, S.F. Yang, Adv. Mater. (2017), http://dx.doi.org/10.1002/adma.201605776.
[71] E.F. Elstner, A. Heupel, Anal. Biochem. 70 (1976) 616–620.
[72] Z.J. Sun, H.F. Zheng, J.S. Li, P.W. Du, Energy Environ. Sci. 8 (2015) 2668–2676.
[73] X.B. Chen, S.H. Shen, L.J. Guo, S.S. Mao, Chem. Rev. 110 (2010) 6503–6570.
[74] S.Q. Liu, Z. Chen, N. Zhang, Z.R. Tang, Y.J. Xu, J. Phys. Chem. C 117 (2013) 8251–8261.
[75] D. Xu, Z.P. Liu, J.B. Liang, Y.T. Qian, J. Phys. Chem. B 109 (2005) 14344–14349.
[76] Y.L. Min, G.Q. He, Q.J. Xu, Y.C. Chen, J. Mater. Chem. A 2 (2014) 2578–2584.
[77] W.L. Zhen, H.B. Gao, B. Tian, J.T. Ma, G.X. Lu, ACS Appl. Mater. Inter. 8 (2016) 10808–10819.